Petroleum Science 23 (2026) 1829–1841

Contents lists available at ScienceDirect

Petroleum Science

journal homepage: www.keaipublishing.com/en/journals/petroleum-science

Original Paper

Physics-informed neural network for reconstruction of seismic data under compressed sensing sampling

Yin-Shuo Li [a], Wen-Kai Lu [a,*], Xiao-Gang Huang [b], Ji-Cai Ding [b], Cao Song [a]

[a] Department of Automation, Tsinghua University, Beijing, 100084, China
[b] China National Offshore Oil Corporation (CNOOC) Research Institute Ltd., Beijing, 100083, China

ARTICLE INFO

Article history:
Received 19 May 2025
Received in revised form
6 November 2025
Accepted 10 November 2025
Available online 23 January 2026

Edited by Meng-Jiao Zhou

Keywords:
Physics-informed neural network
Reconstruction of 3-D seismic data
Move-out transformation
Alias suppression

ABSTRACT

Seismic exploration is one of the most critical methodologies and the highest-cost expenditures in the pre-exploration. The main cost of seismic exploration is acquiring seismic data, which can be significantly reduced through compressed sensing (CS) techniques. Traditional and deep learning (DL) CS methods offer unprecedented opportunities for cost optimization while maintaining data fidelity. However, CS methods rely on random acquisition, which performs poorly when the seismic data are not randomly acquired. This manuscript proposes a novel physics-informed neural network (PINN) framework for reconstructing 3D seismic data acquired via down-sampling from Ocean Bottom Seismometer (OBS) observation systems. The compressed sensing acquisition system of seismic data contains two types of sparsity: 1) 2D random missing traces, 2) Dual random missing of source lines and source points. The proposed method employed move-out (MO) transformations with multiple constant velocities to mitigate aliasing artifacts and improve reconstruction accuracy. Then, a pre-interpolation process is utilized for the MO-transformed seismic data groups. Additionally, a semblance evaluation mechanism dynamically assigns weights to each MO dataset, generating optimized, pre-interpolated seismic profiles. Finally, the PINN architecture integrates physical constraints to refine the reconstructed data. The experimental results demonstrate the superior reconstruction performance and computational efficiency of the proposed method compared with the state-of-the-art.

1. Introduction

Seismic exploration is one of the most critical methodologies in the pre-exploration of oil and gas (Al-Sadi, 1980), whose cost is huge due to the refinement and complexity (Herrmann, 2009). The cost of sampling and processing has limited the scale of application of advanced geological exploration means. Since seismic data acquisition accounts for 60%–80% of seismic exploration costs, compressive sensing (CS) technology is utilized to reduce the acquisition cost (Li et al., 2024). The essence of compressed sensing reconstruction is realizing compression during acquisition. According to the Nyquist sampling theorem (Vaidyanathan, 2002), the sampled signal can retain the complete information in the original signal only if the sampling frequency is more than twice the highest frequency in the signal (Baraniuk and Steeghs, 2017). The compressed sensing theorem has demonstrated that if the signal is sparse in some transform domain, then it can be reconstructed from sampling points far below those required by the sampling theorem. Since seismic signals are sparse in transform domains such as the f–k domain and wavelet domain, seismic data is a satisfactory signal to be reconstructed by compressed sensing (Iqbal et al., 2023; Li et al., 2012).

Compressed sensing technology transforms the observed signal to a sparse domain by an observation matrix and eliminates artifacts in the sparse domain (Tsaig and Donoho, 2006). Its prerequisites are: (1) the data is sparse in a transformation domain, (2) the observation matrix satisfies the restricted isometry property. Traditional compressed sensing methods build the observation matrix and then calculate the target signal in the sparse domain, which can be divided into convex relaxation methods (Gu et al., 2019; Hayden et al., 2016), Bayesian compressed sensing (Ji et al., 2008), and greedy pursuits (Liu and Temlyakov, 2011).

* Corresponding author.
E-mail address: lwkmf@mail.tsinghua.edu.cn (W.-K. Lu).
Peer review under the responsibility of China University of Petroleum (Beijing).

https://doi.org/10.1016/j.petsci.2025.11.023

Convex relaxation methods relax the non-convex problem to a convex problem for solving. Specifically, the ℓ_0 norm optimization objective is relaxed to ℓ_1 norm (Huang et al., 2015) or trace norm (Riofrio et al., 2017). Bayesian compressive sensing method (Babacan et al., 2009) assumes that the signal conforms to some prior distribution (such as a sparse Gaussian distribution) through a probability model, and utilizes maximum a posteriori (MAP) estimation to recover the signal. Greedy pursuit methods, such as matching pursuits (MP) (Do et al., 2008) and Orthogonal MP (Rabah et al., 2014), approximate the sparse solution by progressively selecting the most relevant basis vectors. However, these methods are time-consuming, unstable, and rely on random sampling (Monika et al., 2021).

Compressed sensing includes two steps: (1) compressed sensing sampling, and (2) compressed sensing reconstruction. In lots of production scenarios, such as seismic data acquisition, the observation system has been established, and the sampling process in compressed sensing is inalterable (Gan et al., 2016). Reconstructing complete data from preset randomly sampled results in compressed sensing can be regarded as a reconstruction task. The reconstruction of 3D seismic data with randomly missing source points and source lines in this manuscript aims to reduce the cost of high-precision seismic data acquisition systems. Ocean bottom seismometer (OBS) observation systems, including ocean bottom cable acquisition (Zheng et al., 2011) and ocean bottom node acquisition (Guo et al., 2023), are the typical scene of the CS reconstruction task. The source is from the shot of air guns on the ship, so the cost can be reduced by reducing the number of routes or shots, i.e., reducing source points. As shown in Fig. 1 (a), complete sampling results with high precision are required in the OBS acquisition systems, whose shortage is the huge cost. The random sparse sampling designed in compressed sensing, as shown in Fig. 1(b), can reduce costs, which will cause randomly missing traces due to the loss of source points and source lines. The seismic data is a common receiving point (CRP) gather, while the randomness is consistent for each receiver, which is coupled with Bernoulli samplings (Haas and König, 2004) of traces and lines on the CRP gather. In a certain OBS acquisition system, the pattern is fixed throughout the survey. In the different OBS acquisition system, the patterns are independent and identically distributed. The target of this manuscript is to restore complete sampled seismic data (a) from the observed CS acquisition seismic data (b). Specifically, this manuscript focuses on the reconstruction of seismic data after compressed sensing acquisition, which is also known as interpolation.

Benefiting from the development of neural networks in recent years, the convolutional neural network (CNN) (LeCun et al., 2015) has provided outstanding performance in various signal processing problems such as computer vision. CNN-based methods have achieved outstanding performance in classification (Minaee et al., 2021b), detection (Zhao et al., 2019), and segmentation (Minaee et al., 2021a). Besides, researchers have demonstrated that CNN-based methods can also provide robust and efficient results in pixel-level tasks such as matting (Xu et al., 2017), inpainting (Lugmayr et al., 2022), and super-resolution (Zhang et al., 2023). The target of the seismic signal process is similar to that of images (2D) or videos (3D). Thus, lots of researchers have introduced deep learning (DL) and CNN into seismic signal processing (Li et al., 2020). Furthermore, CNN methods for seismic processes and other tasks in geophysics will achieve better performance if they fuse domain knowledge into the DL network (Li et al., 2021). The target of interpolation of seismic data with uniform missing traces is the same as image super-resolution, while that of seismic data interpolation under randomly missing traces can also be regarded as inpainting. Specifically, the essence of seismic data reconstruction is to reconstruct the unobserved signal from the observed signal (Gan et al., 2016). Wang et al. (2018) have utilized CNN to realize the interpolation of seismic data with uniform missing traces.

The precondition for outstanding performances of DL-based methods in computer vision tasks is plenty of paired high-quality training data. For example, most restoration methods are trained on lots of paired high-quality and low-quality images, where the high-quality images are observed and the low-quality images come from the degradation of high-quality images. However, the requisition of plenty of paired high-quality data is hard to satisfy in seismic interpolation. Thus, researchers propose to solve the problem by synthetic training data, which is limited by the difference between the synthetic and field data (Li et al., 2024). Specifically, these methods are trained on the maps of synthetic data but do not have the generalization ability to apply to field data due to the synthetic data not being independently identically distributed with the field data. Therefore, self-supervised DL methods are proposed to learn the interpolation of seismic data with randomly missing traces. Kong et al. (2020) has proposed to reconstruct the texture structure in seismic data by prior in the network, where the self-supervised DL-based method learns a complete signal from noise. Cao et al. (2022) re-sampled the observed seismic data to build the input and target of the neural network and introduce a partial convolutional neural network

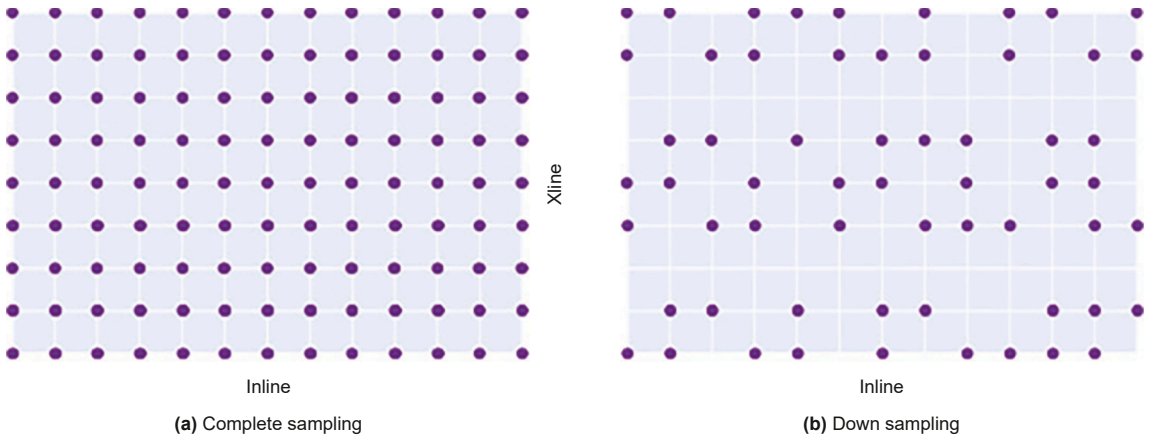

Fig. 1. Schematic diagram of the shot position of the OBS compressive sensing observation system. **(a)** Complete sampling results with high precision. **(b)** Random sparse sampling is designed in compressed sensing, which contains source lines missing and source traces missing.

(PCNN) (Liu et al., 2018) to fill the holes in seismic data with random missing. These self-supervised DL-based methods require plenty of training on the observed field data, which is time-consuming and cannot accomplish the fast processing requirements in seismic data interpolation (Li et al., 2024).

To overcome the above difficulties, Li et al. (2024) have proposed a fast self-supervised DL-based method for compressed sensing reconstruction of seismic data. In the proposed method, 3D gated convolutional neural networks (GCNN) (Yu et al., 2019) are utilized to extract features from seismic data with holes. Besides, a global-local module is employed to extract the global waveform and local texture simultaneously. Li's method has achieved the best performance of 3D seismic data reconstruction under a limited training time, but it requires the observed seismic data to be randomly sampled in two dimensions (Inline and Xline). However, its performance is poor on compressed sensing reconstruction in OBS as shown in Fig. 1 (b) since the observed seismic data contains missing source lines.

To solve the actual production problem in OBS compressed sensing reconstruction, this manuscript proposes a novel physics-informed neural network (PINN) for seismic data reconstruction. The proposed method utilizes move-out (MO) transformations with multiple constant velocities to address aliasing artifacts and enhance reconstruction accuracy, and then a deep neural network is applied to interpolate seismic data after MO. Besides, a physics-informed neural network is employed to fuse the pre-interpolated seismic data and refine the reconstructed results by physical constraints.

2. Theory and methods

This manuscript proposes a novel method based on a physics-informed neural network for seismic data interpolation. As shown in Fig. 2, the input of the proposed pipeline is observed seismic data with randomly missing source points and source lines, while the output is reconstructed seismic data. The pipeline of the proposed method contains move-out (MO), pre-interpolation, inversion of move-out, and post-refine. Besides, compressed sensing acquisition and evaluation of interpolation are utilized in the evaluation.

Since the observed seismic data contains serious aliasing, MO is utilized to render the in-phase axis horizontal. In the OBS observation system, the sources are from the gas guns on the ship, while the receivers are on the ocean bottom. Considering that the sources and receivers are not on the same horizontal plane in OBS, multiple velocities are utilized to obtain a group of MO data with different velocities. Pre-interpolation is utilized in each MO data, and the alias suppression performance of the interpolated results is evaluated by the seismic semblance (Chauris and Farshad, 2023). Besides, the interpolated results are transformed back to seismic data by the inversion MO (iMO) process. The iMO results are weighted and summed with semblance evaluation results, as the weights are the pre-interpolated seismic data. Finally, a physics-informed neural network for 3D reconstruction is proposed for the 3D refiner of the interpolation results, where the velocity energy spectrum is utilized as the physical constraint.

2.1. Move-out

The proposed move-out (MO) transformation is similar to NMO, which aims at flattening the in-phase axis by multiple velocities. The difference between them is that NMO is based on the hyperbolic assumption and is not reversible, while the proposed MO is a linear transformation and is reversible. The expression of MO and iMO is as follows:

$$\begin{cases} \text{MO}: \quad t_k = t - \left\lfloor \left(x^2 + h^2\right)^{0.5} \Big/ v_k \right\rfloor, \\ \text{iMO}: \quad t = t_k + \left\lfloor \left(x^2 + h^2\right)^{0.5} \Big/ v_k \right\rfloor, \end{cases} \tag{1}$$

where x represents offset on the horizontal plane, h denotes depth of the ocean, while t stands for the time. Besides, v_k represents the constant velocity in the k-th MO transformation, while t_k denotes

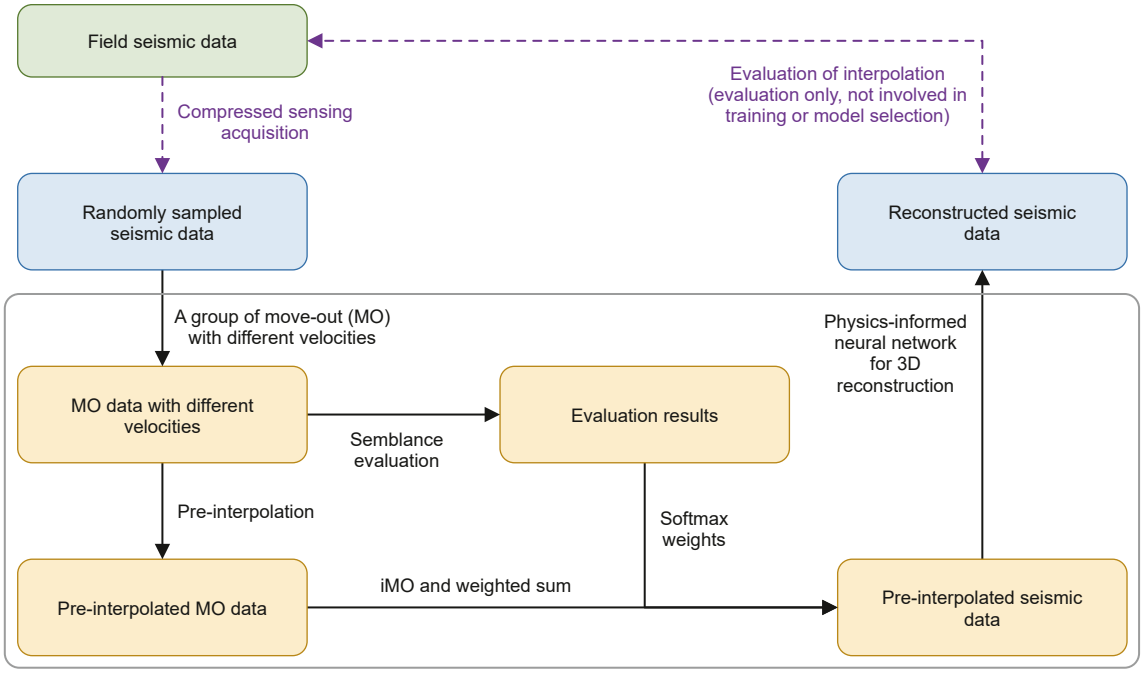

Fig. 2. Pipeline of the proposed method.

the moved time after the MO transformation. Meanwhile, $\lfloor \cdot \rfloor$ stands for the downward rounding, which ensures t_i has the same sampling interval as t.

To simplify the calculation, slowness s is employed to replace the velocity, where $s_k = 1/v_k$. Then, the Eq. (1) can be modified to

$$\begin{cases} \text{MO}: & t_k = t - \left\lfloor \left(x^2 + h^2\right)^{0.5} s_k \right\rfloor, \\ \text{iMO}: & t = t_k + \left\lfloor \left(x^2 + h^2\right)^{0.5} s_k \right\rfloor. \end{cases} \tag{2}$$

As shown in Fig. 3, the direction of the in-phase axis at different positions is different, and the slowness required to eliminate the false frequency is also different, so multiple groups of slowness are needed to eliminate the effect of false frequency. Benefiting from the same time sampling interval, the MO operation is reversible, i.e., $t = f_{\text{iMO}}[f_{\text{MO}}(t)]$.

The proposed MO function is utilized as the transform function to suppress the alias, while the proposed iMO function is applied to convert the seismic data back to the original domain. The expression of MO and iMO functions is as follows:

$$\begin{cases} d_k &= f_{\text{MO}}(d; s_k), \\ d &= f_{\text{iMO}}(d_k; s_k), \end{cases} \tag{3}$$

where d represents the observed seismic data, while d_k denotes the seismic data after MO transformation. Besides, f_{MO} and f_{iMO} are the MO function and iMO function with constant slowness s_k.

2.2. Pre-interpolation

A 3D gated convolution neural network with large convolution kernels is utilized to interpolate the seismic data after MO transformation and obtain the pre-interpolation result. The expression is as follows:

$$\widehat{d}_k = f_1(d_k; \theta_1), \tag{4}$$

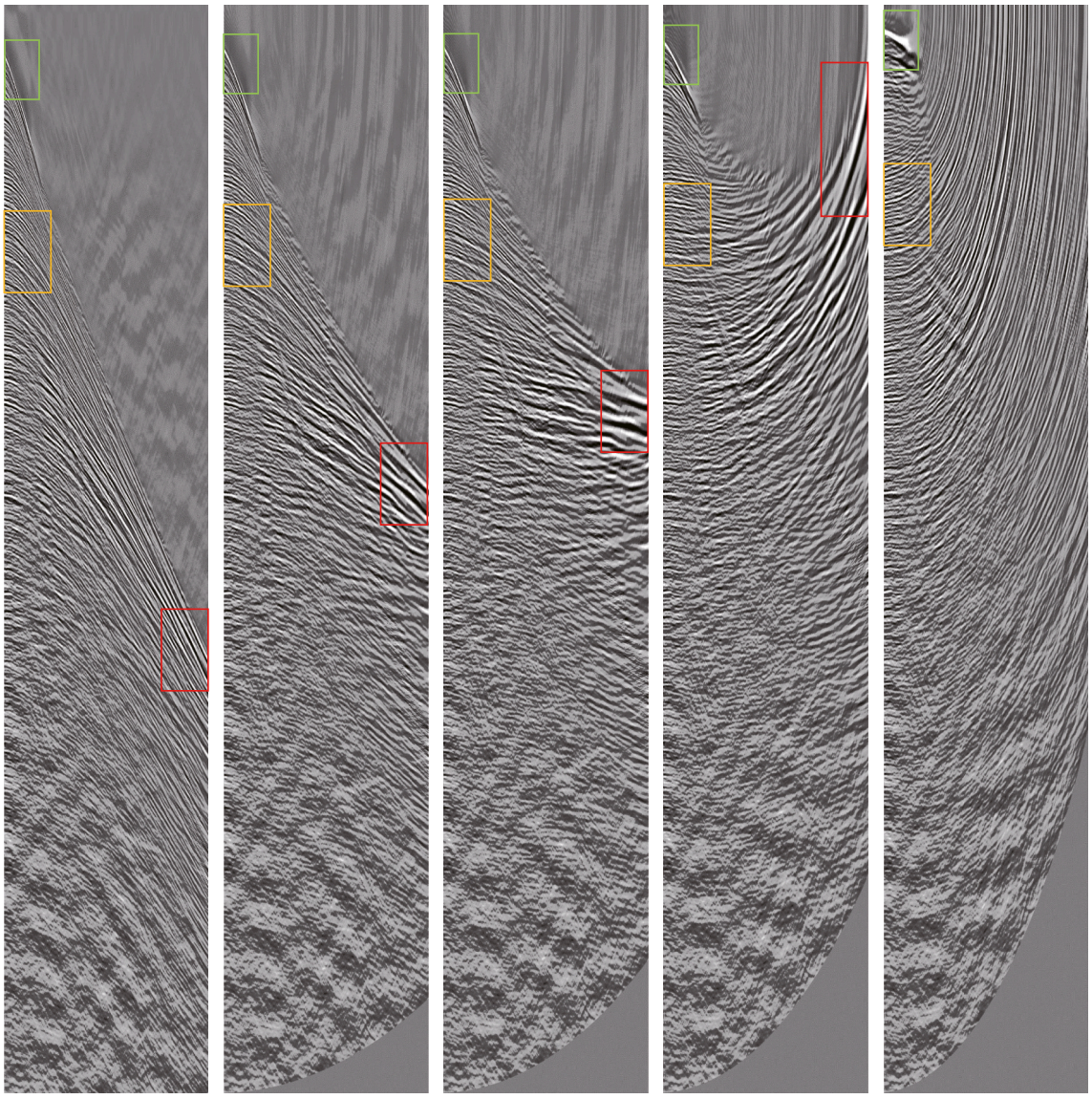

(a) Original **(b)** 0.49 ms/m **(c)** 0.4 ms/m **(d)** 0.5 ms/m **(d)** 0.6 ms/m

Fig. 3. Example of move-out transformation with multiple slowness (velocities).

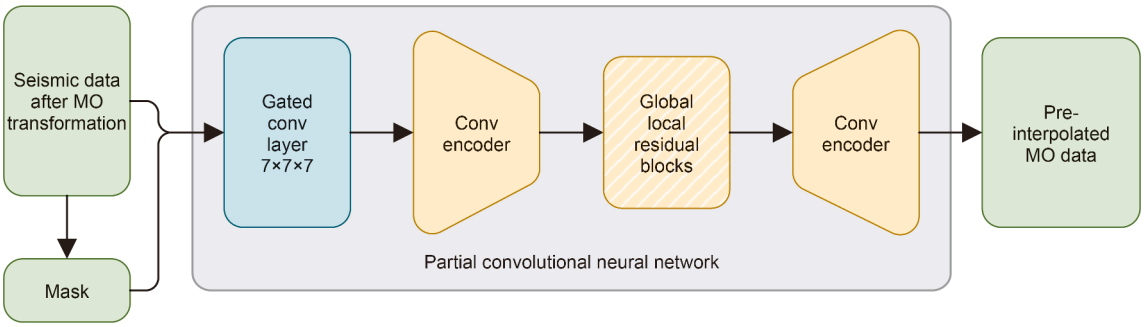

Fig. 4. The structure of the proposed 3D gated convolution neural network with large convolution kernels. The first layer is a partial convolutional layer with kernel size $7 \times 7 \times 7$, which is followed by encoder and decoder modules with 3D convolutional layers. Besides, residual blocks with 3D global-local layers (Li et al., 2024).

where f_1 represents the 3D gated convolution neural network with large convolution kernels, whose parameters are denoted by θ_1. As shown in Fig. 4, the first layer of the pre-interpolation model is a partial convolutional layer with kernel size $7 \times 7 \times 7$, which is followed by encoder and decoder modules with 3D convolutional layers. Besides, residual blocks with 3D global-local layers are proposed by Li et al. (2024). The partial convolutional layer with kernel size $7 \times 7 \times 7$ can repair the missing continuous 3 traces. The proposed 3D gated convolution neural network with large convolution kernels is pre-trained on synthetic and field data without aliases, which aims to fill the random holes in seismic data. Since the model is pre-trained on seismic data without alias, its performance on seismic data without alias will be better in inference. Thus, MO transformations with multiple constant velocities are utilized to find the transformed seismic data without aliases.

The proposed method evaluates the alias suppression effect in each MO data by semblance evaluation. The expression of semblance evaluation f_{oe} is as follows:

$$\varkappa_{k,\tau,i,j} = f_{\text{oe}}\left(d_{k,\tau,i,j}\right) = \frac{\sum_{\tau}\left|\sum_{i,j} d_{k,\tau,i,j}\right|}{\varepsilon + \sum_{\tau,i,j}\left|d_{k,\tau,i,j}\right|}, \tag{5}$$

where τ, i, and j represent the indexes of time, Inline, and Xline in pre-stack seismic data, while k denotes the index of velocity selected in an MO transformation. $\varepsilon = 10^{-12}$ represents a minimal number that prevents the denominator from being 0. Besides, $d_{k,\tau,i,j}$ stands for the seismic data on $[\tau, i, j]$ after MO transformation with slowness s_k, while $\varkappa_{k,\tau,i,j}$ denotes the semblance result of $d_{k,\tau,i,j}$. Meanwhile, $\sum_{\tau,i,j} d_{k,\tau,i,j,k}$ represents the sum of d_k on region $\{\tau \in [\tau - \Delta\tau, \tau + \Delta\tau], i \in [i - \Delta i, i + \Delta i], j \in [j - \Delta j, j + \Delta j]\}$.

For each location $[\tau, i, j]$, the calculated semblance results $\varkappa_k$ are utilized as the weight of $\widehat{d}_k$ to acquire the pre-interpolation result. The expression of pre-interpolation is as follows:

$$\begin{cases} d_k &= f_{\text{MO}}(d; v_k), \\ \widehat{d}_k &= f_1(d_k; \theta_1), \\ \dot{d}_k &= f_{\text{iMO}}(\widehat{d}_k; s_k), \\ \widehat{d} &= \dfrac{\sum_k \dot{d}_k e^{\varkappa_k}}{\sum_k e^{\varkappa_k}}, \end{cases} \tag{6}$$

where $\dot{d}_k$ denotes the pre-interpolated seismic data under MO transformation with v_k. As shown in Eq. (6), SoftMax is utilized to increase the weight of the subset with low alias in all MO transforms in the weighted summation result.

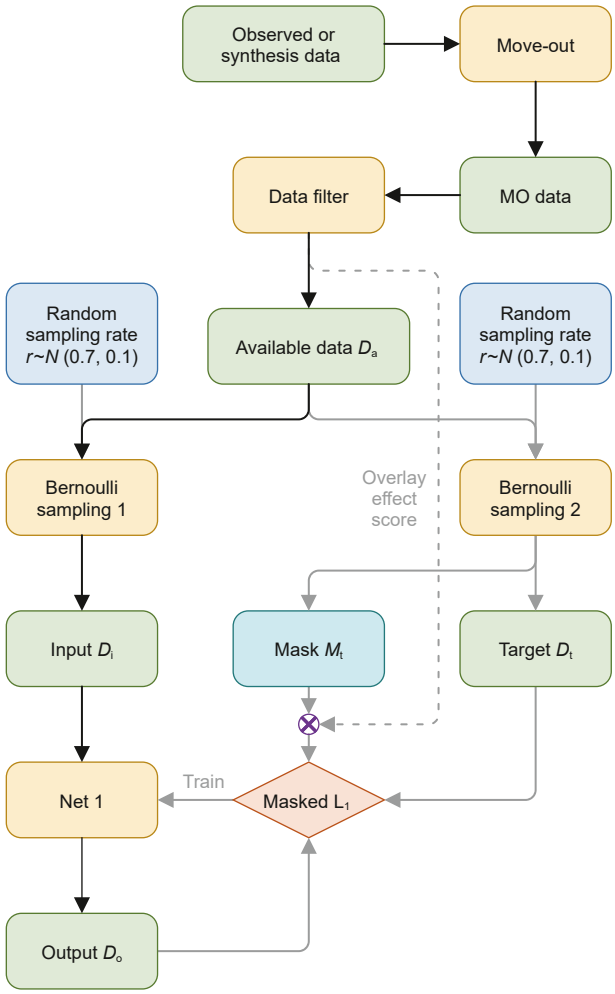

Fig. 5. Pipeline of pre-interpolation model training and testing. The black lines are the pipeline of training and testing, while the gray lines are for training only.

2.3. Offline semi-supervised learn

On the one hand, the proposed 3D gated convolutional neural network for pre-interpolation can be trained offline on the observed data with randomly missing data, which doesn't rely on paired training data. On the other hand, the sample space is extracted and selected by move-out transformation and semblance evaluation, so the neural network for pre-interpolation can learn from any available observed field data or synthetic data. Thus, the training of the proposed pre-interpolation is called offline semi-supervised learning.

As shown in Fig. 5, the training data of the pre-interpolation model is obtained from the field or synthesis data, which can be fully observed or randomly missing. The collected pre-stack seismic data is proposed by move-out transformation, and the MO-processed data is cropped and shaped in 128 × 32 × 128. MO data whose average semblance score $\varkappa$ is larger than $\varkappa_{\text{th}}$ is screened to create training data, which is marked as available data D_a.

While training, the available data D_a is randomly sampled by Bernoulli sampling (Haas and König, 2004) with a random sampling rate $r \sim N(0.7, 0.1)$, where $N(0.7, 0.1)$ denotes a normal distribution with 0.7 as the mean and 0.1 as the standard deviation. Specifically, two independent and identically distributed quadratic random Bernoulli samplings are utilized to generate the input data D_i and target data D_t, respectively. Then, D_i is fed to the pre-interpolation model *Net*1 and the output data D_o. A masked ℓ_1 loss function is employed to calculate the loss and gradient, while the Adam optimizer is applied to update the parameters of *Net*1. The expression of the masked loss function is as follows:

$$\begin{aligned} M &= M_t \odot [\text{ReLU}(\varkappa - \varkappa_{\text{th}}) + \varkappa_{\text{th}}], \\ \mathcal{L} &= \ell_1(D_o \odot M, D_t \odot M), \end{aligned} \tag{7}$$

where $\mathcal{L}$ represents the masked loss function based on ℓ_1 norm, while $\odot$ denotes dot product. The mask of target data D_t is utilized as the mask, which is marked as M_t. Besides, the semblance score $\varkappa$ is dot multiplied with M_t, which works as the weights of points in the loss function. Meanwhile, the semblance score $\varkappa$ that is less than $\varkappa_{\text{th}}$ is set to zero, which is devoted to sieving out the residual alias influence in the training samples.

The black lines are the pipeline of training and testing, while the gray lines are for training only. During evaluation and inference, all MO data is selected in the data filter. Besides, the random sampling rate for Bernoulli sampling 1 is adjusted to 1, which means all available data is selected as the input data, i.e., $D_i = D_a$. Meanwhile, the loss function and target data are not required during the test.

2.4. PINN refine: online self-supervised learn

The pre-interpolated seismic data is further refined by a 3D physics-informed neural network, the expression is as follows:

$$o = f_2(\widehat{d}; \theta_2) \tag{8}$$

where f_2 represents the 3D physics-informed neural network, whose parameters are marked as θ_2. Besides, o denotes the interpolated seismic data. The structure of the proposed 3D physics-informed neural network is similar to the pre-interpolation, where the partial convolutional layer is removed. The proposed 3D physics-informed neural network learns the target seismic data in a self-supervised way.

The loss function of the proposed 3D PINN is as follows:

$$\begin{aligned} &\mathcal{L} = \lambda_1 \ell_1(o \odot m, d), \\ &+\lambda_2 \ell_1\left(o \frac{\sum_1^n m}{n}, d\right), \\ &+\lambda_3 \mathfrak{X}[\mathcal{M}(o), \mathcal{M}(d)], \end{aligned} \tag{9}$$

where $\mathcal{L}$ represents the loss function, ℓ_1 denotes the L_1 norm function, $\odot$ denotes the dot product in the matrices, and m stands for the mask of observed seismic data d. Specifically, seismic data is randomly missing with trace as the smallest unit and $m_{i,j} = 1$ if $d_{i,j}$ is observed, otherwise $m_{i,j} = 0$. Besides, $\mathcal{M}(o) = \sum_{i,j} f_{\text{MO}}(o)$ represents the velocity energy spectrum, which is calculated by the sum in Xline and Inline directions and shaped in $[k, t]$. Meanwhile, $\mathfrak{X}$ stands for cross-correlation loss, and $\lambda_1, \lambda_2, \lambda_3$ denote the weight of sub-loss functions. In Eq. (9), the loss function contains data loss and model loss. $\lambda_1 l_1(o \odot m, x)$ denotes the data loss, while the model loss contains energy loss $\lambda_2 \ell_1(o \frac{\sum_1^n m}{n}, d)$ and velocity energy spectrum cross-correlation loss $\lambda_3 \mathfrak{X}[\mathcal{M}(o), \mathcal{M}(d)]$.

3. Experiments

In this section, the implementation details of the proposed method are described, including the parameter setting and hardware information. Besides, the proposed method is evaluated on the synthetic and field data with different kinds of missing distributions.

3.1. Implementation details

The training data of the pre-interpolation model is obtained from the field or synthesis data, which can be fully observed or randomly missing. The collected pre-stack seismic data is proposed by move-out transformation, and the MO-processed data is cropped and shaped in 128 × 32 × 128. Cropped MO data whose average semblance score $\varkappa$ is larger than 0.3 is screened to create training data. Besides, the pixel level semblance threshold $\varkappa_{\text{th}}$ is set to 0.3. The initial learning rate is 10^{-4}, which will be down to 80% of the current value every 10 epochs. The weight parameters in Eq. (9) are set to $\lambda_1 = 1$, $\lambda_2 = 0.3$, $\lambda_3 = 0.3$. The set of MO velocities (slowness) is calculated as follows: 1) find the maximum slowness s_x that can flatten the in-phase axis with the maximum inclination angle; 2) uniformly insert several speed values between 0 and s_x. The interval size depends on the amount of video memory and the size of the GPU. Smaller intervals and more velocities will result in higher performance and increased resource consumption. The semblance (overlay effect) threshold is utilized to filter the obtained data to obtain high-quality training data. We have set the value to 0.3 to ensure the training data is clean. The targets of each loss function are the same, i.e., reconstructing the missing traces with the same distribution as the observed traces. Thus, the method is not sensitive to the weights. Since the first fraction is a more direct constraint, λ_1 is larger than λ_2 and λ_3, while λ_2 is the same as λ_3. The proportion of λ_2 and λ_1 can be 0.1 ~ 0.3.

All experiments are conducted on a Ubuntu system server with a 13th Gen Intel(R) Core(TM) i9-13900K central processing unit (CPU) and two Nvidia GeForce RTX 4090 graphics processors (GPU). The setting of parameters and hardware provided above is an example utilized in this manuscript, but it is not a necessary condition for the proposed method to achieve satisfactory results. The signal-to-noise ratio (SNR) is utilized to evaluate the reconstruction performance of the proposed method and the contrast methods. The expression of SNR is as follows:

$$\text{SNR} = 10\log_{10}\frac{\text{signal}^2}{\text{noise}^2} = 10\log_{10}\frac{y^2}{(x-y)^2} \tag{10}$$

where y denotes the ground truth (GT) of the signal and x represents the reconstruction results, which can be regarded as the sum of the GT signal and noise.

For comparative analysis, five representative methods spanning conventional and deep learning paradigms are selected as contrasts: (1) traditional reconstruction methods including the Directional Difference Tensor Factorization (DDTF) (Yu et al., 2015) and Damped Multichannel Singular Spectrum Analysis (DMSSA) (Chen et al., 2016); (2) the deep image prior-based approach (DIP)

(Kong et al., 2020) and 3D partial convolutional neural network (PCNN) (Cao et al., 2022) as two representative deep learning implementations; (3) the state-of-the-art 3D gated convolutional Neural Network (GCNN) (Li et al., 2024) for benchmarking against cutting-edge developments. The DL-based contrast methods are online self-supervised methods, and the authors have suggested training their methods for a limited time. Thus, this manuscript has also compared the proposed method with the contrast DL-based method under limited training time.

3.2. Synthetic experiments under 2D random sampling

The proposed method and the contrast methods are evaluated on synthetic data from the Sandia/SEG Salt Model 45 shot subset, whose time sampling interval is 8 ms. The cropped data is shaped in [174, 30, 160], where the dimension order is [time, line, inline]. Fig. 6(a) shows the ground-truth (GT) of the cropped Sandia/SEG Salt Model, while Fig. 6(b) provides the compressed sensing observation result with randomly 60% missing traces. DDTF is a

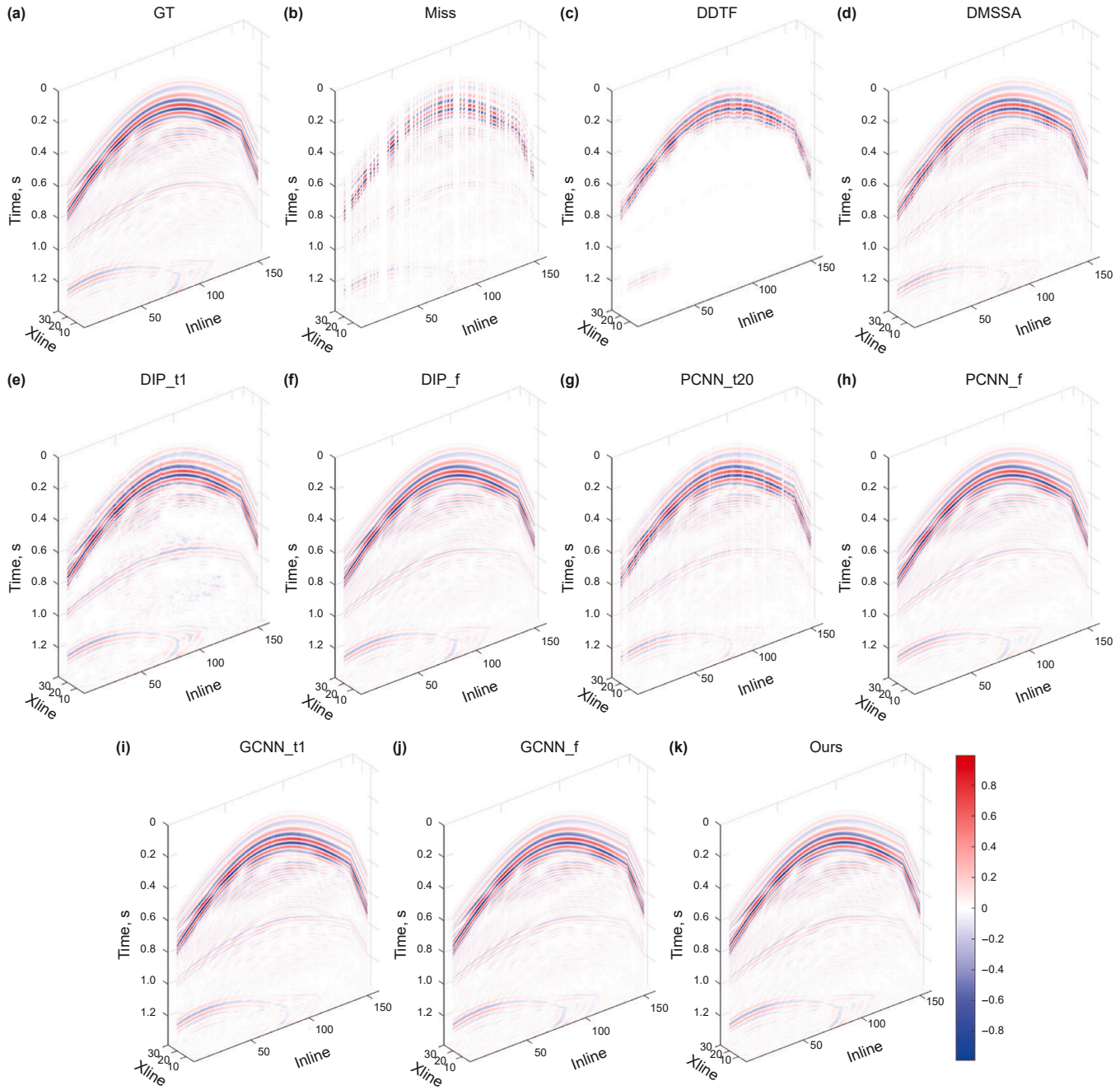

Fig. 6. Visual qualitative of reconstruction results of the proposed method and contrasts on synthetic data from Sandia with randomly 60% missing traces. **(a)** The fully observed ground truth (GT). **(b)** The compressed sensing of (a) with randomly 60% missing traces. **(c)**–**(k)** The reconstructed results of DDTF (Yu et al., 2015), DMSSA (Chen et al., 2016), DIP (Kong et al., 2020), PCNN (Cao et al., 2022), GCNN (Li et al., 2024), and the proposed method.

fast traditional compressed sensing reconstruction method, but its performance is poor. As shown in Fig. 6 (c), DDTF can only reconstruct primary waves, which are powerless to deal with waveforms. For example, DDTF has failed to reconstruct texture details from 0.8 s to 1.2 s. As shown in Fig. 6 (d), DMSSA is another traditional method, which obtains better performance with more time consumption. The training time of the limited training experiments of online self-supervised DL-based methods is marked according to the time cost of DDTF. For example, DIP_t1 denotes the training time of DIP is the same as the operation time of DDTF, and PCNN_t20 means the training time of PCNN is 20 times as long as DDTF. The performance of DIP_t1, PCNN_t20, and GCNN_t1 are shown in Fig. 6(e), (g), (i), which are better than DDTF but not well enough. Fig. 6(f), (h), (j) provides the reconstruction results of fully trained DIP, PCNN, and GCNN, although they have obtained outstanding performance, all of them are with high time consumption. The performance of the proposed method is shown in Fig. 6(k), which demonstrates that the proposed method can achieve outstanding performance without plenty of self-supervised training.

Another synthetic dataset based on the field data from the South China Sea is utilized to evaluate the proposed method. The time sampling interval is 1.5 ms, and the number of grids in the Inline, Xline, and time dimensions is 64, 32, and 192, respectively. The fully observed seismic data is sampled with 40% randomly missing traces. Fig. 7(a) and (b) provide the ground truth and observed data with 40% randomly missing traces. Besides, Fig. 7 shows the reconstruction results of DMSSA (Chen et al., 2016), GCNN (Li et al., 2024), and the proposed method. Since the missing rate is low and the main waveform direction is unidirectional, all methods can observe visually satisfactory results.

3.3. Field experiments under 2D random sampling

The proposed method and contrast methods are further compared on field data from the South China Sea. The grid of observed seismic data in the Xline direction is less (8 lines), while the number of grids in the Inline and time directions is 472 and 480. Besides, the time sampling interval is 2 ms. As shown in Fig. 8 (a), the field data is full of details under different angles. Fig. 8(b) provides the simulated compressed sensing acquisition result with 50%. And Fig. 8(c)–(k): the reconstructed results of DDTF (Yu et al., 2015), DMSSA (Chen et al., 2016), limited DIP (Kong et al., 2020), fully trained DIP, limited PCNN (Cao et al., 2022), fully trained PCNN, limited GCNN (Li et al., 2024), fully trained GCNN, and the proposed method. The reconstruction results of traditional methods (DDTF and DMSSA), limited DIP, and limited PCNN cannot obtain visually satisfying performance, while the reconstruction results of fully trained DIP and PCNN are better than them. Besides, the performances of GCNN and the proposed method are similar to the ground truth, and it is difficult to determine which one is better by visual qualitative analysis.

Table 1 shows the quantitative evaluation of the performance of the proposed method and the contrasts between synthetic data and field data. Synthetic data 1 in Table 1 is the data shown in Fig. 6, while another synthetic is the synthetic data based on the field data from the South China Sea. Table 1 has demonstrated that the proposed method can achieve the best performance with a fast speed on both synthetic and field data. Specifically, the proposed method can obtain performances better than those of DL-based methods with full training. Besides, the time cost of the proposed method is less than that of the DL-based methods under limited training. Thus, the proposed method is better than traditional and state-of-the-art (SOTA) DL-based reconstruction methods on compressed sensing sampling under 2D randomly missing traces.

3.4. Experiments on OBS observation system under dual random samplings

The above experiments have demonstrated that the proposed method is better than traditional and DL-based reconstruction methods on compressed sensing sampling under 2D randomly missing traces. In more familiar field scenes, such as the OBS CS observation system shown in Fig. 1, the CS observation is based on dual random missing traces. The dual random missing contains the missing of source lines and source points. The proposed methods are further evaluated on this kind of CS reconstruction task.

Fig. 9 provides the visual qualitative reconstruction results of the proposed method and contrasts the synthetic data from Sandia

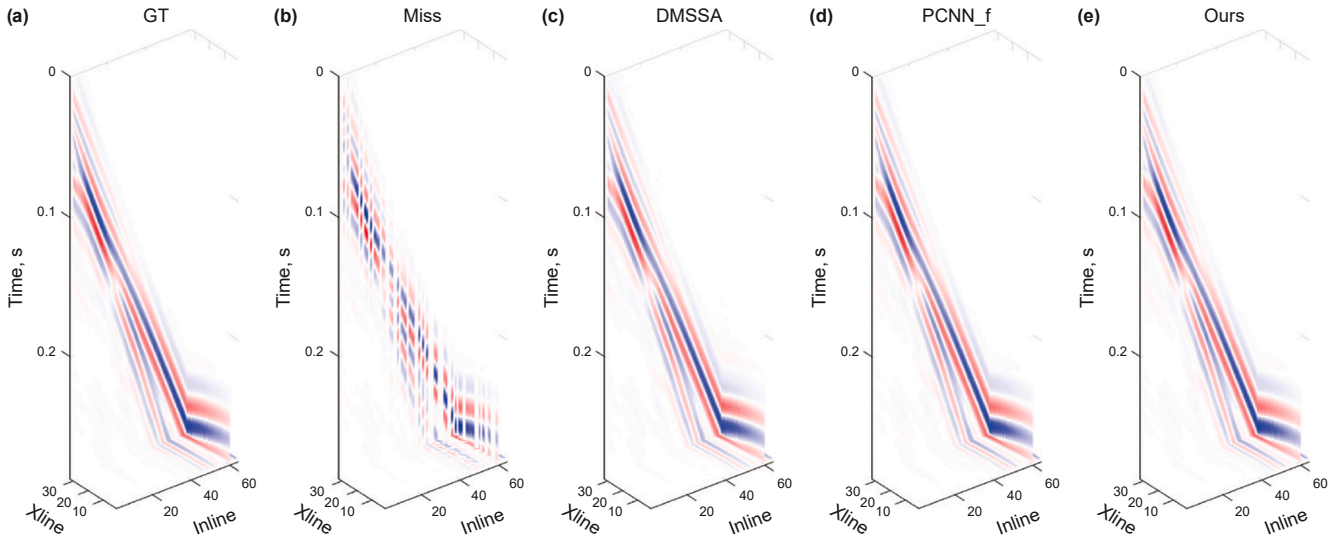

Fig. 7. Visual qualitative reconstruction results of the proposed method and contrasts on synthetic data based on field data from the South China Sea with randomly 40% missing traces. **(a)** The fully observed ground truth (GT). **(b)** The compressed sensing of (a) with randomly 40% missing traces. **(c)**–**(e)** The reconstructed results of DMSSA (Chen et al., 2016), GCNN (Li et al., 2024), and the proposed method.

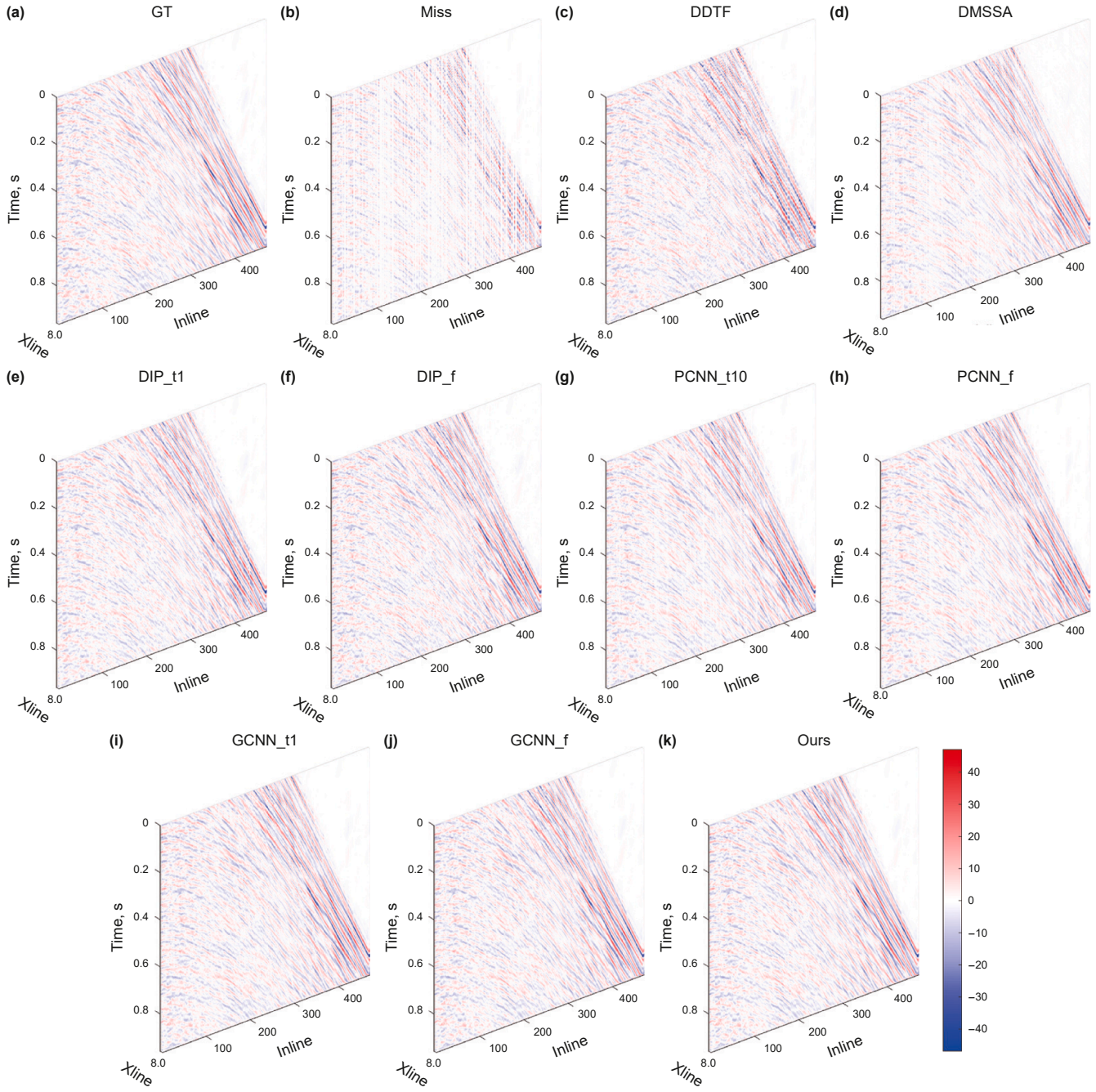

Fig. 8. Visual qualitative of reconstruction results of the proposed method and contrasts on field data from the South China Sea with randomly 50% missing traces. **(a)** The fully observed ground truth (GT). **(b)** The compressed sensing of (a) with randomly 60% missing traces. **(c)**–**(k)** The reconstructed results of DDTF (Yu et al., 2015), DMSSA (Chen et al., 2016), DIP (Kong et al., 2020), PCNN (Cao et al., 2022), GCNN (Li et al., 2024), and the proposed method.

with randomly 60% missing traces. The randomly missing contains two processes: 1) randomly missing source lines (whole "Inline", 1D randomly missing) with 40% miss rate; 2) randomly missing source points (2D randomly missing) with 33.3% miss rate. Thus, the sampling rate of the compressed sensing acquisition is $(1\%-40\%)\cdot(1\%-33.3\%)=40\%$. Fig. 9(a) shows a 2D slice of the fully observed ground truth (GT), which is not sampled on the compressed sensing sampling. Besides, Fig. 9(b)–(d) provides the reconstructed results of DMSSA (Chen et al., 2016), GCNN (Li et al., 2024), and the proposed method on the missing line shown in (a). It has been demonstrated that traditional and DL-based reconstruction methods can reconstruct mainly waves under dual random samplings. Besides, the performance of DMSSA and GCNN under dual random samplings is worse than that of these methods under 2D random sampling. Furthermore, the proposed method can overcome the challenge of dual random sampling and achieve the SOTA performance.

The visual comparison of the experiment on field data under dual randomly missing is shown in Fig. 10, where the ground truth is the same as that of Fig. 8. The dual randomly missing contains 25% randomly missing source lines and another 33.3% missing source points. As shown in Fig. 10(b)–(c), the performances of DMSSA and GCNN on dual randomly missing tasks are unsatisfactory. Specifically, the reconstruction results of these two

Table 1
Quantitative evaluation of the performance of the proposed method and the contrasts. The comparison is implemented in terms of signal-to-noise ratio (SNR, higher is better) and time cost (lower is better). Meanwhile, synthetic data 1 and 2 are randomly down-sampled with 60% and 40% missing traces, while the missing ratio of field data is 50%. The training time of X_l is limited, while X_f is fully trained. The time cost of traditional methods is the total execution time, while that of self-supervised methods is the online training time. Besides, the time cost of the proposed method only contains the online refinement time, since the pre-training is the training process in the supervised DL-based method.

Method	Synthetic 1		Synthetic 2		Field	
	SNR ↑	Time ↓	SNR ↑	Time ↓	SNR ↑	Time ↓
Miss (LQ)	2.21 dB	–	3.83 dB	–	3.11 dB	–
DDTF	5.70 dB	63 s	7.38 dB	31 s	6.43 dB	388 s
DMSSA	12.15 dB	4803 s	21.62 dB	2031 s	8.92 dB	6997 s
DIP_l	10.79 dB	80 s	14.00 dB	34 s	9.28 dB	388 s
DIP_f	23.32 dB	8327 s	15.19 dB	4267 s	11.10 dB	6483 s
$PCNN_l$	11.16 dB	1260 s	21.29 dB	620 s	10.05 dB	3880 s
$PCNN_f$	23.94 dB	21.2 h	29.75 dB	10.7 h	13.16 dB	10.5 h
$GCNN_l$	18.11 dB	63 s	27.81 dB	30 s	11.76 dB	388 s
$GCNN_f$	24.85 dB	2335 s	31.13 dB	1169 s	13.23 dB	1608 s
Ours	26.29 dB	15 s	32.37 dB	7 s	14.57 dB	11 s

methods fail to reconstruct the texture details, and the energies of the reconstruction results are inconsistent with those of the ground truth. The performance of these methods on dual randomly missing tasks is worse than that of these two methods on single 2D randomly missing tasks. Differently, Fig. 10(d) has demonstrated that the proposed method can achieve outstanding performance on dual randomly missing.

Table 2 provides the quantitative evaluation of the performance of the proposed method and the contrasts. The comparison is implemented in terms of signal-to-noise ratio (SNR, higher is better). Besides, in the single randomly missing situation, synthetic data 1 and 2 are randomly down-sampled with 60% and 40% missing traces, while the missing ratio of field data is 50%. Meanwhile, the missing rate in the synthetic 1 in dual randomly missing task contains 40% missing lines and 33.3% missing points,

Table 2
Quantitative evaluation of the performance of the proposed method and the contrasts. The comparison is implemented in terms of signal-to-noise ratio (SNR, higher is better). Besides, in the single randomly missing situation, synthetic data 1 and 2 are randomly down-sampled with 60% and 40% missing traces, while the missing ratio of field data is 50%. Meanwhile, the missing rate in the synthetic 1 in dual randomly missing task contains 40% missing lines and 33.3% missing points, so the missing rate is $1-(1-40\%)(1-33.3\%)=60\%$, which is marked as 40%&33.3% → 60%. The missing rates of synthetic data 2 and field data are 20%&25% → 40% and 25%&33.3% → 50%.

Method	Synthetic 1		Synthetic 1		Field	
	Single	Dual	Single	Dual	Single	Dual
Miss	2.21 dB	2.09 dB	3.83 dB	3.61 dB	3.11 dB	2.95 dB
DMSSA	12.15 dB	10.13 dB	21.62 dB	18.37 dB	8.92 dB	7.76 dB
GCNN_f	24.85 dB	18.97 dB	31.13 dB	24.46 dB	13.23 dB	8.24 dB
Ours	26.29 dB	25.53 dB	32.37 dB	31.54 dB	14.57 dB	13.79 dB

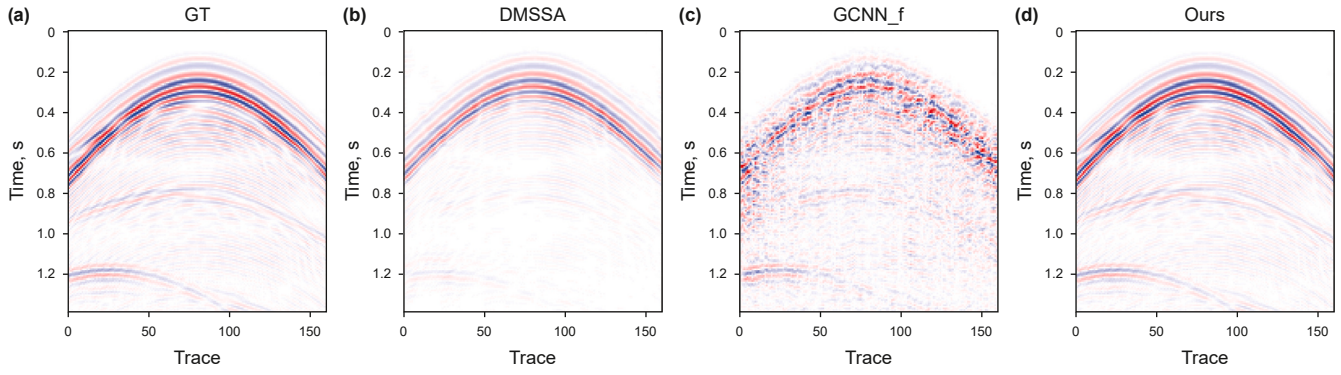

Fig. 9. Visual qualitative reconstruction results of the proposed method and contrasts on synthetic data from Sandia with dual random sampling. The randomly missing contains two processes: 1) Randomly missing source lines (whole "Inline") with 40% miss rate; 2) Randomly missing source points with 33.3% miss rate. **(a)** A 2D slice of the fully observed ground truth (GT), which is not sampled on the compressed sensing sampling. **(b)**–**(d)** The reconstructed results of DMSSA (Chen et al., 2016), GCNN (Li et al., 2024), and the proposed method on the missing line are shown in (a).

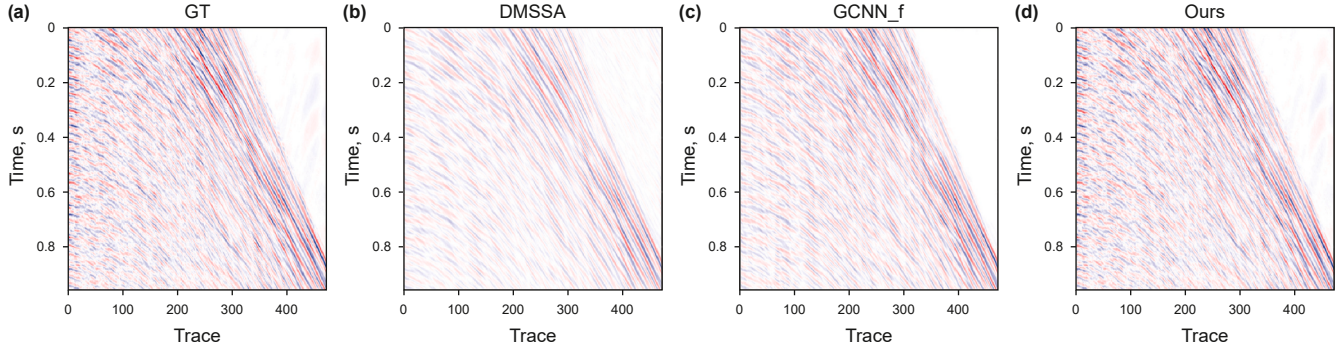

Fig. 10. Visual qualitative of reconstruction results of the proposed method and contrasts on field data from the South China Sea with dual random sampling. The randomly missing contains two processes: 1) randomly missing source lines (whole "Inline") with 25% miss rate; 2) randomly missing source points with 33.3% miss rate. **(a)** A 2D slice of the fully observed ground truth (GT), which is not sampled on the compressed sensing sampling. **(b)**–**(d)** The reconstructed results of DMSSA (Chen et al., 2016), GCNN (Li et al., 2024), and the proposed method on the missing line are shown in (a).

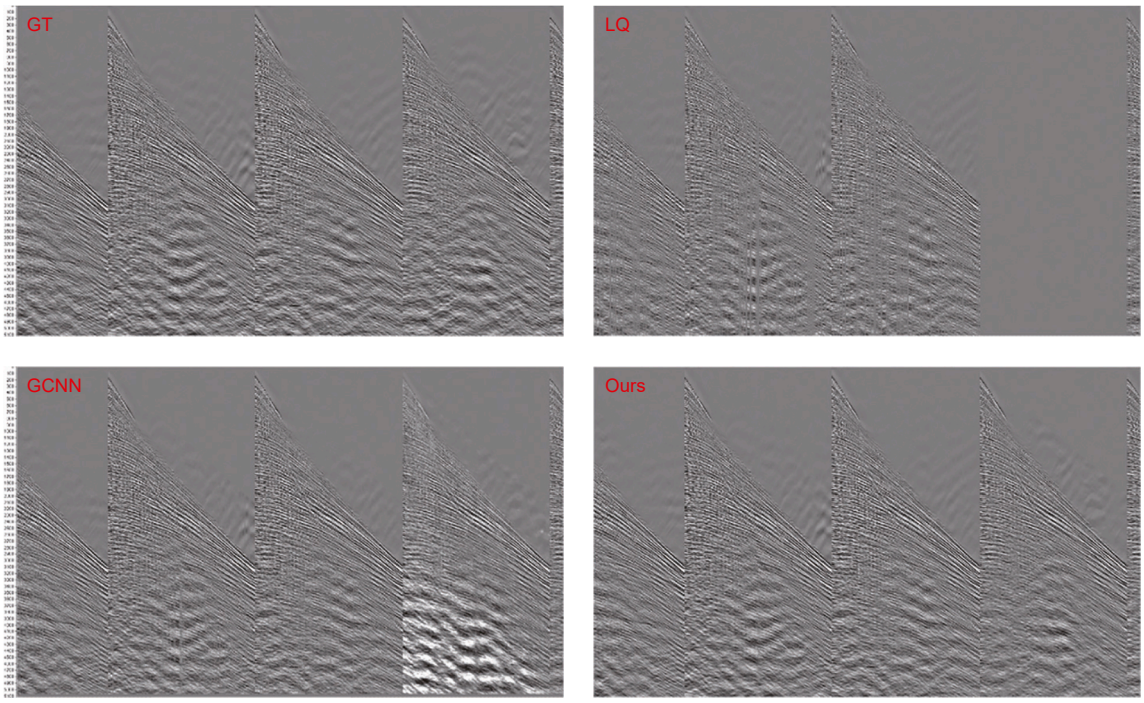

Fig. 11. Visual qualitative of reconstruction results of the proposed method and GCNN on another field data from the South China Sea with dual random sampling. The randomly missing contains randomly missing source lines and randomly missing source points, while the total missing rate is 49%. **(a)** The fully observed ground truth (GT). **(b)** The observed seismic data under compressed sensing acquisition. **(c)**–**(d)** The reconstructed results of GCNN (Li et al., 2024) and the proposed method.

so the missing rate is $1-(1-40\%)(1-33.3\%)=60\%$, which is marked as 40%&33.3% → 60%. Furthermore, the missing rates of synthetic data 2 and field data are 20%&25% → 40% and 25%&33.3% → 50%. The time cost of each method on each data is the same as that in Table 1. As shown in Table 2, the SNR of dual randomly missing results is slightly less than that of single missing results. However, the reconstruction results of DMSSA and GCNN on dual randomly missing tasks are significantly worse than those of DMSSA and GCNN on single randomly missing tasks. Besides, the quantitative evaluation shown in Table 2 has demonstrated that the proposed method can achieve the best performance on both single 2D randomly missing traces and dual randomly missing on source lines and source points.

Fig. 11 provides visual qualitative reconstruction results of the proposed method and GCNN on another field data from the South China Sea with dual random sampling. The grid numbers of the seismic data in time, Inline, and Xline direction are 4000, 205, and 72, while the sampling rate of time is 2 ms. The randomly missing contains randomly missing source lines and randomly missing source points, while the total missing rate is 49% and the SNR is 4.38 dB. GCNN has successfully reconstructed the missed points in partially sampled source lines, but failed to reconstruct the missed source line; the SNR of GCNN's output is 7.28 dB. Besides, the proposed method has provided outstanding performance on the reconstruction of missed source points and source lines, the SNR of whose reconstruction result is 11.06 dB.

3.5. Ablation study

An ablation study is further designed to demonstrate the necessity of each process. Three ablation methods are utilized to evaluate the importance of the two PINN processes, which include MO and refining.

- Abl1 denotes the contrast without the two PINN processes (MO and refining).
- Abl2 represents the contrast without MO.
- Abl3 stands for the contrast without refining.

These methods are evaluated on the above four data sets under dual random sampling.

Table 3 provides the quantitative evaluation results on the ablation study under dual random sampling. The comparison is implemented in terms of signal-to-noise ratio (SNR, higher is better). The missing rate in synthetic 1 contains 40% missing lines and 33.3% missing points, so the missing rate is $1-(1-40\%)(1-33.3\%)=60\%$, which is marked as 40%&33.3% → 60%. The missing rates of synthetic data 2, field data 1, and field data 2 are 20%&25% → 40%, 25%&33.3% → 50%, and 25%&32% → 49%. As shown in Table 3, the proposed method has achieved the best performance on the test data, which demonstrates that both the MO and refining are important for reconstruction. Besides, the comparison of Abl1, Abl2, and Abl3 proved that both the MO and refine are effective, and the MO process plays a more important role.

Table 3
Quantitative evaluation for ablation study under dual random sampling. The comparison is implemented in terms of signal-to-noise ratio (SNR, higher is better). The missing rate in synthetic 1 contains 40% missing lines and 33.3% missing points, so the missing rate is $1-(1-40\%)(1-33.3\%)=60\%$, which is marked as 40%&33.3% → 60%. The missing rates of synthetic data 2, field data 1, and field data 2 are 20%&25% → 40%, 25%&33.3% → 50%, and 25%&32% → 49%.

Method	Structure		Synthetic		Field	
	MO	Refiner	Syn 1	Syn 2	Field 1	Field 2
Miss	–	–	2.09 dB	3.61 dB	2.95 dB	4.38 dB
Abl1	×	×	12.67 dB	19.82 dB	7.78 dB	6.39 dB
Abl2	×	✓	19.65 dB	25.24 dB	8.61 dB	7.50 dB
Abl3	✓	×	25.02 dB	30.93 dB	13.46 dB	10.74 dB
Ours	✓	✓	25.53 dB	31.54 dB	13.79 dB	11.06 dB

4. Conclusion

This manuscript has proposed a novel physics-informed neural network (PINN) framework for reconstructing 3D seismic data acquired via down-sampling from the Ocean Bottom Seismometer (OBS) observation system. The proposed method employed move-out (MO) transformations with multiple constant velocities to mitigate aliasing artifacts and improve reconstruction accuracy. Then, a pre-interpolation process is utilized for the MO-transformed seismic data groups. Additionally, a semblance evaluation mechanism dynamically assigns weights to each MO dataset, generating optimized, pre-interpolated seismic profiles. Finally, the PINN architecture integrates physical constraints to refine the reconstructed data. The pre-interpolation model is trained on plenty of unpaired data in a semi-supervised way, while the refined model learns on the target data in a self-supervised way. The proposed method can deal with single 2D randomly missing traces and dual randomly missing source lines and source points. The experiments have demonstrated that the proposed method can achieve state-of-the-art (SOTA) performance on both single 2D randomly missing and dual randomly missing tasks on field and synthetic data.

CRediT authorship contribution statement

Yin-Shuo Li: Writing – review & editing, Writing – original draft, Methodology, Formal analysis, Conceptualization. **Wen-Kai Lu:** Resources, Project administration, Funding acquisition, Data curation, Conceptualization. **Xiao-Gang Huang:** Project administration, Data curation. **Ji-Cai Ding:** Data curation. **Cao Song:** Project administration.

Declaration of competing interest

The authors declare that they have no known competing financial interests or personal relationships that could have appeared to influence the work reported in this paper.

Acknowledgements

This research is financially supported by the NSFC National Major Scientific Research Instrument Development Project (Department Recommendation, Grant No. 42327901).

References

Al-Sadi, H.N., 1980. Seismic exploration. J. Can. Soc. Explor. Geophys. 1, 13–43. https://doi.org/10.1007/978-3-642-02332-3_17.

Babacan, S.D., Molina, R., Katsaggelos, A.K., 2009. Bayesian compressive sensing using laplace priors. IEEE Trans. Image Process. 19 (1), 53–63. https://doi.org/10.1109/TIP.2009.2032894.

Baraniuk, R.G., Steeghs, P., 2017. Compressive sensing: A new approach to seismic data acquisition. Lead. Edge. 36 (8), 642–645. https://doi.org/10.1190/tle36080642.1.

Cao, W., Shi, Y., Wang, W., Guo, X., Tian, F., Zhao, Y., 2022. Self-supervised multitask 3-d partial convolutional neural network for random noise attenuation and reconstruction in 3-d seismic data. IEEE Trans. Geosci. Rem. Sens. 60, 1–19. https://doi.org/10.1109/TGRS.2022.3225923.

Chauris, H., Farshad, M., 2023. Seismic differential semblance-oriented migration velocity analysis—status and the way forward. Geophysics 88, U81–U100. https://doi.org/10.1190/geo2021-0661.1.

Chen, Y., Huang, W., Zhang, D., Chen, W., 2016. An open-source matlab code package for improved rank-reduction 3d seismic data denoising and reconstruction. Comput. Geosci. 95, 59–66. https://doi.org/10.1016/j.cageo.2016.06.017.

Do, T.T., Gan, L., Nguyen, N., Tran, T.D., 2008. In: Sparsity adaptive matching pursuit algorithm for practical compressed sensing. IEEE, pp. 581–587. https://doi.org/10.1109/ACSSC.2008.5074472.

Gan, S., Wang, S., Chen, Y., Chen, X., Huang, W., Chen, H., 2016. Compressive sensing for seismic data reconstruction via fast projection onto convex sets based on seislet transform. J. Appl. Geophys. 130, 194–208. https://doi.org/10.1016/j.jappgeo.2016.03.033.

Gu, B., Chen, Y., Liu, X., Zhou, F., Jiang, R., 2019. Distributed convex optimization compressed sensing method for sparse planar array synthesis in 3-D imaging sonar systems. IEEE J. Ocean. Eng. 45, 1022–1033. https://doi.org/10.1109/JOE.2019.2914983.

Guo, Y., Lin, R., Sacchi, M.D., 2023. Optimal seismic sensor placement based on reinforcement learning approach: an example of obn acquisition design. IEEE Trans. Geosci. Rem. Sens. 61, 1–12. https://doi.org/10.1109/TGRS.2023.3247593.

Haas, P.J., König, C., 2004. A bi-level bernoulli scheme for database sampling. In: Proceedings of the 2004 ACM SIGMOD International Conference on Management of Data, pp. 275–286. https://doi.org/10.1145/1007568.1007601.

Hayden, D., Chang, Y.H., Goncalves, J., Tomlin, C.J., 2016. Sparse network identifiability via compressed sensing. Automatica 68, 9–17. https://doi.org/10.1016/j.automatica.2016.01.008.

Herrmann, F.J., 2009. Sub-Nyquist sampling and sparsity: How to get more information from fewer samples. In: SEG Technical Program Expanded Abstracts 2009, pp. 3410–3415. https://doi.org/10.1190/1.3255570

Huang, X., Liu, Y., Shi, L., Van Huffel, S., Suykens, J.A., 2015. Two-level 1 minimization for compressed sensing. Signal Process 108, 459–475. https://doi.org/10.1016/j.sigpro.2014.09.028.

Iqbal, N., Masood, M., Alfarraj, M., Waheed, U.B., 2023. Deep seismic CS: A deep learning assisted compressive sensing for seismic data. IEEE Trans. Geosci. Rem. Sens. 61, 1–9. https://doi.org/10.1109/TGRS.2023.3289917.

Ji, S., Xue, Y., Carin, L., 2008. Bayesian compressive sensing. IEEE Trans. Signal Process. 56, 2346–2356. https://doi.org/10.1109/TSP.2007.914345.

Kong, F., Picetti, F., Lipari, V., Bestagini, P., Tang, X., Tubaro, S., 2020. Deep prior-based unsupervised reconstruction of irregularly sampled seismic data. IEEE Geoscience and Remote Sensing Letters 19, 1–5. https://doi.org/10.1109/LGRS.2020.3044455.

LeCun, Y., Bengio, Y., Hinton, G., 2015. Deep learning. Nature 521, 436–444. https://doi.org/10.1038/nature14539.

Li, C., Mosher, C.C., Kaplan, S.T., 2012. Interpolated compressive sensing for seismic data reconstruction. In: SEG Technical Program Expanded Abstracts 2012, segam2012-1335.1. https://doi.org/10.1190/segam2012-1335.1

Li, Y., Cao, W., Lu, W., Huang, X., Ding, J., Song, C., 2024. Reconstruct 3-D seismic data with randomly missing traces via fast self-supervised deep learning. IEEE Trans. Geosci. Rem. Sens. 62, 1–14. https://doi.org/10.1109/TGRS.2024.3401130.

Li, Y., Song, J., Lu, W., Monkam, P., Ao, Y., 2020. Multitask learning for super-resolution of seismic velocity model. IEEE Trans. Geosci. Rem. Sens. 59, 8022–8033. https://doi.org/10.1109/TGRS.2020.3034502.

Li, Y., Song, J., Lu, W., Monkam, P., Ao, Y., 2021. Super-resolution of seismic velocity model guided by seismic data. IEEE Trans. Geosci. Rem. Sens. 60, 1–12. https://doi.org/10.1109/TGRS.2021.3075622.

Liu, G., Reda, F.A., Shih, K.J., Wang, T.C., Tao, A., Catanzaro, B., 2018. Image inpainting for irregular holes using partial convolutions. In: Proceedings of the European Conference on Computer Vision (ECCV), pp. 85–100. https://doi.org/10.1007/978-3-030-01252-6_6.

Liu, E., Temlyakov, V.N., 2011. The orthogonal super greedy algorithm and applications in compressed sensing. IEEE Trans. Inf. Theor. 58, 2040–2047. https://doi.org/10.1109/TIT.2011.2177632.

Lugmayr, A., Danelljan, M., Romero, A., Yu, F., Timofte, R., Van Gool, L., 2022. Repaint: Inpainting using denoising diffusion probabilistic models. In: Proceedings of the IEEE/CVF Conference on Computer Vision and Pattern Recognition, pp. 11461–11471.

Minaee, S., Boykov, Y., Porikli, F., Plaza, A., Kehtarnavaz, N., Terzopoulos, D., 2021a. Image segmentation using deep learning: A survey. IEEE Trans. Pattern Anal. Mach. Intell. 44 (7), 3523–3542. https://doi.org/10.1109/TPAMI.2021.3059968.

Minaee, S., Kalchbrenner, N., Cambria, E., Nikzad, N., Chenaghlu, M., Gao, J., 2021b. Deep learning–based text classification: A comprehensive review. ACM Comput. Surv. 54 (3), 1–40. https://doi.org/10.1145/343972.

Monika, R., Samiappan, D., Kumar, R., 2021. Adaptive block compressed sensing – A technological analysis and survey on challenges, innovation directions and applications. Multimed. Tool. Appl. 80, 4751–4768. https://doi.org/10.1007/s11042-020-09932-0.

Rabah, H., Amira, A., Mohanty, B.K., Almaadeed, S., Meher, P.K., 2014. Fpga implementation of orthogonal matching pursuit for compressive sensing reconstruction. IEEE Trans. Very Large Scale Integr. Syst. 23, 2209–2220. https://doi.org/10.1109/TVLSI.2014.2358716.

Riofrio, C.A., Gross, D., Flammia, S.T., Monz, T., Nigg, D., Blatt, R., Eisert, J., 2017. Experimental quantum compressed sensing for a seven-qubit system. Nat. Commun. 8, 15305–15312. https://doi.org/10.1038/ncomms15305.

Tsaig, Y., Donoho, D.L., 2006. Extensions of compressed sensing. Signal Process 86, 549–571. https://doi.org/10.1016/j.sigpro.2005.05.029.

Vaidyanathan, P., 2002. Generalizations of the sampling theorem: seven decades after nyquist. IEEE Transactions on Circuits and Systems I: Fundamental Theory and Applications 48, 1094–1109. https://doi.org/10.1109/81.948437.

Wang, B., Zhang, N., Lu, W., Zhang, P., Geng, J., 2018. Seismic data interpolation using deep learning based residual networks. In: 80th EAGE Conference and Exhibition 2018. https://doi.org/10.3997/2214-4609.201801394.

Xu, N., Price, B., Cohen, S., Huang, T., 2017. Deep image matting. In: Proceedings of the IEEE Conference on Computer Vision and Pattern Recognition, pp. 2970–2979.

Yu, J., Lin, Z., Yang, J., Shen, X., Lu, X., Huang, T.S., 2019. Free-form image inpainting with gated convolution. In: Proceedings of the IEEE/CVF International Conference on Computer Vision, pp. 4471–4480.

Yu, S., Ma, J., Zhang, X., Sacchi, M.D., 2015. Interpolation and denoising of high-dimensional seismic data by learning a tight frame. Geophysics 80 (5), V119–V132. https://doi.org/10.1190/geo2014-0396.1.

Zhang, Y., Zhang, K., Chen, Z., Li, Y., Timofte, R., Zhang, J., Zhang, K., Peng, R., Ma, Y., Jia, L., et al., 2023. Ntire 2023 challenge on image super-resolution (×4): Methods and results. In: Proceedings of the IEEE/CVF Conference on Computer Vision and Pattern Recognition, pp. 1864–1883.

Zhao, Z.Q., Zheng, P., Xu, S.T., Wu, X., 2019. Object detection with deep learning: A review. IEEE Transact. Neural Networks Learn. Syst. 30 (11), 3212–3232. https://doi.org/10.1109/TNNLS.2018.2876865.

Zheng, Y., Barton, P., Singh, S., 2011. Strategies for elastic full waveform inversion of time-lapse ocean bottom cable (OBC) seismic data. In: SEG Technical Program Expanded Abstracts 2011, pp. 4195–4200. https://doi.org/10.1190/1.3628083.